Mode-mode competition and unstable behavior in a homogeneously broadened ring laser

L. M. Narducci and J. R. Tredicce*
Physics Department, Drexel University, Philadelphia, Pennsylvania 19104

L. A. Lugiato
Dipartimento di Fisica, Università degli Studi di Milano, I-20133 Milano, Italy

N. B. Abraham and D. K. Bandy
Physics Department, Bryn Mawr College, Bryn Mawr, Pennsylvania 19010
(Received 3 June 1985)

We present theoretical and experimental evidence for a new type of multimode instability in a homogeneously broadened ring-laser system. The unstable behavior discussed in this paper is the result of multimode competition and can manifest itself either through self-pulsing or hysteretic behavior of the bistable type in the laser output intensity and operating frequency. We have verified some of our predictions with the help of a CO_2 laser whose observed bistable behavior is in good qualitative agreement with the theoretical predictions.

I. INTRODUCTION

The evolution of a multimode laser is a problem of considerable complexity because of the large number of dynamical variables and system parameters that may affect its behavior.[1-3] Even when the optical resonator is designed to support only a single transverse mode, several longitudinal modes can be excited even at moderate pump levels, so that different optical frequencies may coexist in the output field. Normally, under these conditions the output intensity is expected to display a complicated modulation that reflects the competition of the various oscillating modes and the degrees of their mutual entrainment.[4]

There is considerable experimental evidence that inhomogeneously broadened gain lines tend to favor the development of multimode action; on the other hand, also homogeneously broadened lasers, such as CO_2 or high-pressure gas lasers, can be affected by mode-mode competition. In spite of the fact that significant efforts have already been devoted to the analysis of this problem,[4] a complete physical picture of the evolution of a multimode system is still lacking, mainly because of the large number of factors that can influence its behavior. Numerical studies have clarified some qualitative features of the observed dynamical patterns,[4(a)] but have been unable, in general, to provide sufficient information on the physical origin of the breakdown of stability. The situation is complicated by the simultaneous occurrence of single and multimode instabilities (especially with inhomogeneously broadened systems) which makes it very difficult to unambiguously sort out the role of the various dynamical variables that become involved in the evolution.[5]

In an attempt to get to the root of at least some of these problems, it is best to focus our attention on the simplest possible laser model which is capable of multimode operation with the least number of additional complications. For this reason, we propose to investigate the dynamical evolution of a multimode unidirectional ring laser with a homogeneously broadened atomic profile. We ignore the effects of the transverse-field distribution, in spite of its expected relevance for a quantitative comparison with the experiments,[6] and we limit our considerations to optical cavities with high reflectivity mirrors and to active media with a low enough gain per pass so that we may take advantage of the so-called mean-field approximation.[7] The exclusion of counter-propagating fields inside the resonator will remove the complications associated with spatial hole burning and, in general, with a spatially modulated gain profile, while the mean-field condition will enable us to focus on the stability properties of longitudinally uniform steady states. On the other hand, we allow for an arbitrary detuning between the center of the atomic line and a selected reference cavity mode, as well as for an arbitrary intermode spacing.

The chosen physical setting is very similar to the one analyzed in the pioneering contributions by Risken and Nummedal[8] and by Graham and Haken;[9] a significant departure is provided by the extra degree of freedom afforded by our choice of a variable detuning parameter. In addition, unlike these earlier studies, we consider the stability of all the possible steady states (usually, more than one stationary configuration can be supported by the equations of motion) and analyze their behavior as the center of the atomic line is progressively detuned away from the selected reference cavity mode.

In some simple instances, it is intuitively clear what must be expected; for example, if the intermode separation is sufficiently large, a single longitudinal mode should be active under resonant conditions. Upon increasing the detuning its intensity should decrease steadily until this mode is driven below threshold, and laser action stops. For larger values of the detuning, the nearest-neighbor mode, eventually, should turn itself on, go through an emission maximum, and then switch itself off, in turn. In general, of course, the situation may be more complicated.

One of the advantages of the model selected in this study is that the behavior of a single-mode system is well

understood,[10] at least with respect to its response to small perturbations around steady state. Furthermore, when dealing with high-reflectivity mirrors and intermode spacings of at most a few gain linewidths, one is unavoidably involved with good-cavity systems (as we show explicitly in the main text), so that single-mode instabilities are automatically ruled out.[11] In addition, a detailed linear-stability analysis can be developed without excessive complications, and the destabilization mechanisms can be traced out rather easily. Finally, the evolution equations can be solved under the guidance of the linear-stability analysis. In this way, we can focus directly on the combinations of system parameters that can be expected to yield significant dynamical features. These can be analyzed in greater depth with the help of both homodyne and heterodyne spectral techniques to visualize the role of the competing modes in creating the observed output patterns.

In our study, we use the term *"instability"* to denote the occurrence of conditions leading to both discontinuous variations of the steady-state output intensity, and long-term output modulation, upon changing some of the control parameters. According to this nonmenclature, our results indicate that a multimode homogeneously broadened laser may display unstable behavior leading to self-pulsing or hysteresis even under conditions where the single-mode approximation would predict a stable configuration.

The appearance of hysteretic behavior is a new feature of this model, but also the self-pulsing instability, while apparently similar in character to that uncovered in earlier studies,[8,9,12] emerges out of a different physical mechanism, at least for certain ranges of control parameters. In fact, in resonance, an instability of the Risken-Nummedal-Graham-Haken (RNGH) type[8,9] is triggered by the eigenvalue of the linearized problem which is most closely related to the mode-pulled field-amplitude mode. Out of resonance, hysteresis and output pulsations evolve as a result of a phase instability (the so-called phase eigenvalue develops a positive real part). This is reminiscent of the results presented by Gerber and Buttiker,[13] with the important difference that in this case we drop the resonance condition between the center of the atomic line and one of the cavity modes. Thus, in our context, we can offer a clear prescription with regard to the experimental parameters that are to be varied, and predict the occurrence of unstable behavior with the simple application of a detuning scan.[14]

In Sec. II we describe the basic equations of motion and their possible steady states. In Sec. III we summarize the results of our linear-stability analysis. In Sec. IV we display numerical evidence for the predicted instability with the help of time-dependent solutions and their associate power spectra. We conclude in Sec. V, with a discussion of recent experimental work that confirms the theoretical expectations.

II. DESCRIPTION OF THE MODEL AND STEADY-STATE SOLUTION

Our study has its premises in the usual Maxwell-Bloch equations for an active collection of two-level atoms interacting with a traveling electromagnetic wave whose (scalar) electric field has the form

$$E(z,t)=\mathscr{E}(z,t)e^{i(k_R z-\omega_R t)}+\text{c.c.}\ . \tag{2.1}$$

$\mathscr{E}(z,t)$ is the slowly varying complex amplitude, ω_R is an arbitrary reference frequency to be properly selected in the most convenient way, and $k_R=\omega_R/c$. In the following, we select ω_R as one of the cavity eigenfrequencies $\omega_{\bar{n}}=2\pi c\bar{n}/\mathscr{L}$, where $\mathscr{L}$ is the length of the entire ring cavity, and we denote $\omega_{\bar{n}}$ by ω_C.

The equations of motion have the well-known form

$$\frac{\partial\mathscr{F}}{\partial z}+\frac{1}{c}\frac{\partial\mathscr{F}}{\partial t}=-\alpha\mathscr{P}\ , \tag{2.2a}$$

$$\frac{\partial\mathscr{P}}{\partial t}=\gamma_\perp[\mathscr{F}\mathscr{D}-(1+i\tilde{\delta}_{AC})\mathscr{P}]\ , \tag{2.2b}$$

$$\frac{\partial\mathscr{D}}{\partial t}=-\gamma_{||}[\tfrac{1}{2}(\mathscr{F}^*\mathscr{P}+\mathscr{F}\mathscr{P}^*)+\mathscr{D}+1]\ , \tag{2.2c}$$

where

$$\mathscr{F}(z,t)\equiv\mu\mathscr{E}(z,t)/[2\hbar(\gamma_\perp\gamma_{||})^{1/2}]\ ,$$

μ is the modulus of the atomic dipole moment, $\mathscr{P}(z,t)$ is the complex atomic polarization per atom, and $\mathscr{D}(z,t)$ is the difference between the ground- and excited-state occupation probabilities; $\gamma_\perp$ and $\gamma_{||}$ are the polarization and atomic-inversion relaxation rates, respectively, α is the unsaturated gain coefficient per unit length, and $\tilde{\delta}_{AC}=(\omega_A-\omega_C)/\gamma_\perp$ is the dimensionless detuning parameter between the center of the atomic gain line ω_A and the cavity frequency ω_C. The model is completed by appropriate boundary conditions which, in the case of a ring-cavity resonator, take the form

$$\mathscr{F}(0,t)=R\mathscr{F}(L,t-(\mathscr{L}-L)/c)\ , \tag{2.3}$$

where L is the length of the active medium and R is the amplitude reflectivity of the two mirrors; the remaining optical surfaces that are needed to complete the ring are assumed to be ideal reflectors, for simplicity.

The possible stationary states of the system have the form

$$\mathscr{F}(z,t)=\mathscr{F}_{\text{st}}(z)e^{-i\delta\omega t}\ , \tag{2.4a}$$

$$\mathscr{P}(z,t)=\mathscr{P}_{\text{st}}(z)e^{-i\delta\omega t}\ , \tag{2.4b}$$

$$\mathscr{D}(z,t)=\mathscr{D}_{\text{st}}(z)\ , \tag{2.4c}$$

where $\mathscr{F}_{\text{st}}$, $\mathscr{P}_{\text{st}}$, and $\mathscr{D}_{\text{st}}$ are solutions of the equations

$$\frac{d\mathscr{F}_{\text{st}}}{dz}-i\frac{\delta\omega}{c}\mathscr{F}_{\text{st}}=-\alpha\mathscr{P}_{\text{st}}\ , \tag{2.5a}$$

$$0=\mathscr{F}_{\text{st}}\mathscr{D}_{\text{st}}-(1+i\tilde{\Delta})\mathscr{P}_{\text{st}}\ , \tag{2.5b}$$

$$0=\tfrac{1}{2}(\mathscr{F}^*_{\text{st}}\mathscr{P}_{\text{st}}+\mathscr{F}_{\text{st}}\mathscr{P}^*_{\text{st}})+\mathscr{D}_{\text{st}}+1\ , \tag{2.5c}$$

and where the detuning parameter $\tilde{\Delta}$ is defined as

$$\tilde{\Delta}=\tilde{\delta}_{AC}-\delta\omega/\gamma_\perp\ . \tag{2.6}$$

The atomic variables can be determined at once as functions of the stationary field profile

$$\mathscr{P}_{st}(z)=-\mathscr{F}_{st}(z)\frac{1-i\tilde{\Delta}}{1+\tilde{\Delta}^2+|\mathscr{F}_{st}(z)|^2}, \tag{2.7a}$$

$$\mathscr{D}_{st}(z)=-\frac{1+\tilde{\Delta}^2}{1+\tilde{\Delta}^2+|\mathscr{F}_{st}(z)|^2}, \tag{2.7b}$$

while $\mathscr{F}_{st}(z)$ is the solution of Eqs. (2.5a) and (2.7a) subject to the boundary conditions

$$\mathscr{F}_{st}(0)=R\mathscr{F}_{st}(L)e^{i\delta\omega(\mathscr{L}-L)/c}. \tag{2.8}$$

It is convenient to represent the field amplitude in terms of its modulus and phase[15]

$$\mathscr{F}_{st}(z)=\rho(z)e^{i\theta(z)}, \tag{2.9}$$

where $\rho(z)$ and $\theta(z)$ are solutions of the equations

$$\frac{d\rho}{dz}=\frac{\alpha\rho}{1+\tilde{\Delta}^2+\rho^2}, \tag{2.10a}$$

$$\frac{d\theta}{dz}=-\frac{\alpha\tilde{\Delta}}{1+\tilde{\Delta}^2+\rho^2}+\frac{\delta\omega}{c}. \tag{2.10b}$$

Equations (2.10) can be combined to yield the first integral

$$\ln\left[\frac{\rho(z)}{\rho(0)}\right]=-\frac{1}{\tilde{\Delta}}\left[\theta(z)-\theta(0)-\frac{\delta\omega}{c}z\right], \tag{2.11a}$$

while Eq. (2.10a) gives immediately

$$(1+\tilde{\Delta}^2)\ln\left[\frac{\rho(z)}{\rho(0)}\right]+\tfrac{1}{2}[\rho^2(z)-\rho^2(0)]=\alpha z. \tag{2.11b}$$

In addition, the boundary conditions (2.8), expressed in terms of modulus and phase, provide the two constraining relations

$$\rho(0)=R\rho(L), \tag{2.12a}$$

$$\theta(L)-\theta(0)=-\delta\omega\frac{\mathscr{L}-L}{c}+2\pi j, \tag{2.12b}$$

where j is, *a priori*, equal to zero or any positive or negative integer. After combining Eqs. (2.11), (2.12), and (2.6), one readily arrives at the required result

$$\rho_j^2(L)=\frac{2}{1-R^2}[\alpha L-(1+\tilde{\Delta}_j^2)|\ln R|], \tag{2.13a}$$

$$\tilde{\Delta}_j=\tilde{\delta}_{AC}-\delta\omega_j/\gamma_\perp, \tag{2.13b}$$

$$\frac{\delta\omega_j}{\gamma_\perp}=\frac{\tilde{\kappa}\tilde{\delta}_{AC}+j\tilde{\alpha}_1}{1+\tilde{\kappa}}, \tag{2.13c}$$

where

$$\tilde{\alpha}_1=\frac{2\pi c}{\mathscr{L}\gamma_\perp}, \qquad \tilde{\kappa}=\frac{c|\ln R|}{\mathscr{L}\gamma_\perp}. \tag{2.14}$$

The parameter $\tilde{\alpha}_1$ measures the intermode spacing in units of $\gamma_\perp$, while $\tilde{\kappa}$ is the scaled cavity damping rate; the operating frequencies of the stationary solutions are equispaced and given by the mode-pulling formula

$$\omega_c+\delta\omega_j=\frac{(\omega_c+j\alpha_1)\gamma_\perp+\omega_A\kappa}{\gamma_\perp+\kappa}. \tag{2.15}$$

It is clear from Eq. (2.13a) that the threshold condition $\rho_j^2(L)\geq 0$ is satisfied, in general, by more than one steady-state configuration, depending on the gain parameter and the cavity losses. We now focus our attention on a selection of parameters such that

$$\alpha L\to 0, \quad R\to 1 \tag{2.16a}$$

with

$$2C\equiv\frac{\alpha L}{|\ln R|}<\infty. \tag{2.16b}$$

In this limit (mean-field limit[7]) the longitudinal intensity profile along the active medium becomes uniform, and the stationary field configuration is specified by Eqs. (2.13b) and (2.13c) and by

$$|\mathscr{F}_{st}^{(j)}|^2=2C-(1+\tilde{\Delta}_j^2). \tag{2.17}$$

The atomic steady-state variables are given by Eqs. (2.7), as usual.

The results of the stationary analysis are illustrated in Figs. 1(a) and 1(b) for two typical selections of parame-

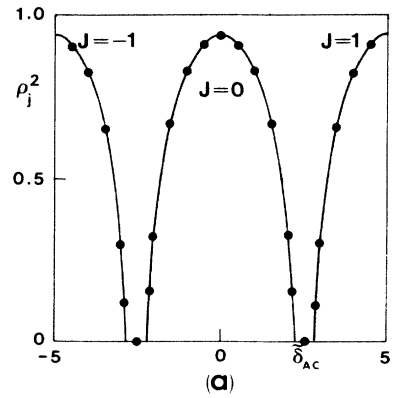

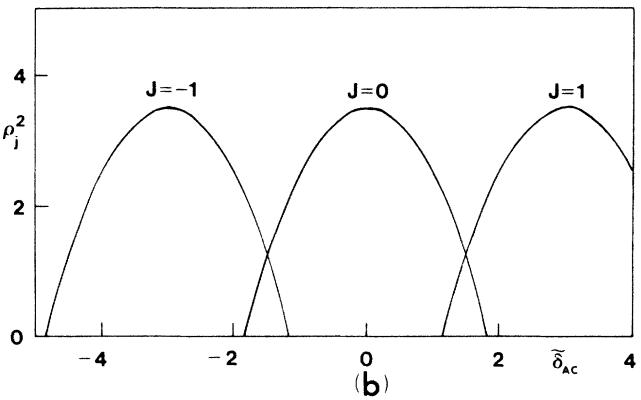

FIG. 1. (a) Steady-state output intensity $\rho_j^2(L)$ [Eq. (2.13)] for the stationary states labeled $j=0,\pm1$ as a function of the detuning parameter $\tilde{\delta}_{AC}$. The value $\tilde{\delta}_{AC}=0$ corresponds to the cavity mode whose frequency ω_c is selected as a reference. The dots correspond to values obtained by direct integration of the space-time–dependent Maxwell-Bloch equations. The parameters used in this calculation are $\alpha L=2$, $R=0.5$, $\tilde{\gamma}=2$, $\tilde{\alpha}_1=5$. (b) Steady-state output intensity $\rho_j^2(L)$ $(J=0,\pm1)$ for $\alpha L=2$, $R=0.5$, and $\tilde{\alpha}_1=3$.

ters. With reference to Fig. 1(a), the physical situation is one in which the center of the atomic line is initially resonant with the cavity mode ω_C, with the output intensity at its largest value consistent with the chosen gain parameter C. As ω_A is gradually detuned away from ω_C (to the right of ω_C, for example), the stationary output intensity decreases, until eventually the steady state $j=0$ falls below threshold. For larger values of the detuning, another steady state ($j=1$ in this case) becomes active; the output intensity begins to grow again and achieves a new maximum when the detuning parameter becomes as large as a free spectral range (the frequency spacing between adjacent modes). The same situation develops, of course, if one carries out a detuning scan to the left of ω_C.

Figure 1(b) differs from Fig. 1(a) only because the free spectral range is now smaller. In this case, two different steady-state configurations coexist, above threshold, for a certain range of detuning parameters. The actual behavior of the system in the presence of competing steady states must be clarified with the help of linear-stability considerations. This is the objective of Sec. III.

III. LINEAR STABILITY ANALYSIS

If the ring-laser system is initially in one of its possible steady states, the short-term evolution that follows a small deviation from the stationary solution is governed by a set of five linearized partial differential equations. Thus, the problem is intrinsically infinite dimensional. The calculation of the rate constants that characterize the linear response is greatly simplified by a procedure that transforms the infinite-dimensional matrix of the linearized problem to a block-diagonal form. Each elementary matrix to be diagonalized leads to a fifth-degree characteristic polynomial equation whose complex roots are the required eigenvalues. Because the structure of the elementary matrices is the same for each of the blocks into which the original problem has been decomposed all the necessary eigenvalues can be determined from a unique routine.

Our procedure has already been detailed in Ref. 16; here we summarize the basic steps. First, we define a new set of independent variables[7]

$$z'=z\ , \qquad t'=t+\frac{\mathscr{L}-L}{c}\frac{z}{L}\ , \tag{3.1}$$

and the new field and atomic variables

$$F(z',t')=\mathscr{F}(z',t')\exp\left[\frac{z'}{L}\ln R\right]\ , \tag{3.2a}$$

$$P(z',t')=\mathscr{P}(z',t')\exp\left[\frac{z'}{L}\ln R\right]\ , \tag{3.2b}$$

$$D(z',t')=\mathscr{D}(z',t')\ . \tag{3.2c}$$

The objective of the transformation (3.1) is to make the boundary conditions (2.3) isochronous (i.e., to eliminate the time delay in the new reference frame), while the transformation (3.2a) has the effect of eliminating the multiplicative factor R, so that the new boundary conditions take the form

$$F(0,t')=F(L,t')\ , \tag{3.3}$$

which is common, for example, of one-dimensional linear vibrations problems.

In the mean-field limit, the Maxwell-Bloch equations for the new field and atomic variables become

$$\frac{\partial F}{\partial t'}+\frac{cL}{\mathscr{L}}\frac{\partial F}{\partial z'}=-\kappa(F+2CP)\ , \tag{3.4a}$$

$$\frac{\partial P}{\partial t'}=\gamma_\perp[FD-(1+i\tilde{\delta}_{AC})P]\ , \tag{3.4b}$$

$$\frac{\partial D}{\partial t'}=-\gamma_{\|}[\tfrac{1}{2}(F^*P+FP^*)+D+1]\ , \tag{3.4c}$$

where

$$\kappa=\frac{c\,|\ln R\,|}{\mathscr{L}}\simeq\frac{cT}{\mathscr{L}} \tag{3.5}$$

and where T is the transmittivity coefficient of the mirrors ($T=1-R$). We now introduce the modal decomposition

$$\begin{bmatrix}F(z',t')\\P(z',t')\end{bmatrix}=e^{-i\,\delta\Omega t'}\sum_{n=-\infty}^{+\infty}e^{ik_nz'}e^{-i\alpha_nt'}\begin{bmatrix}f_n(t')\\p_n(t')\end{bmatrix}\ , \tag{3.6a}$$

$$D(z',t')=\sum_{n=-\infty}^{+\infty}e^{ik_nz'}e^{-i\alpha_nt'}d_n(t')\ ,$$

and

$$\begin{bmatrix}F^*(z',t')\\P^*(z',t')\end{bmatrix}=e^{i\,\delta\Omega t'}\sum_{n=-\infty}^{+\infty}e^{-ik_nz'}e^{i\alpha_nt'}\begin{bmatrix}f_n^*(t')\\p_n^*(t')\end{bmatrix}\ , \tag{3.6b}$$

where $\delta\Omega$ is to be calculated from the steady-state equation and the selection

$$k_n=\frac{2\pi n}{L}\quad(n=0,\pm1,\ldots)$$

automatically ensures the validity of the boundary conditions. The modal amplitudes $f_n, f_n^*, \ldots, d_n$ obey the coupled equations of motion:

$$\dot{f}_n=i\,\delta\Omega f_n-\kappa(f_n+2Cp_n)\ , \tag{3.7a}$$

$$\dot{f}_n^*=-i\,\delta\Omega f_n^*-\kappa(f_n+2Cp_n^*)\ , \tag{3.7b}$$

$$\dot{p}_n=\gamma_\perp\left\{\sum_{n'}f_{n'}d_{n-n'}-\left[1+i\left[\tilde{\delta}_{AC}-\frac{\delta\Omega}{\gamma_\perp}-\tilde{\alpha}_n\right]\right]p_n\right\}\ , \tag{3.7c}$$

$$\dot{p}_n^*=\gamma_\perp\left\{\sum_{n'}f_{n'}^*d_{n-n'}^*-\left[1-i\left[\tilde{\delta}_{AC}-\frac{\delta\Omega}{\gamma_\perp}-\tilde{\alpha}_n\right]\right]p_n^*\right\}\ , \tag{3.7d}$$

$$\dot{d}_n=i\alpha_nd_n-\gamma_{\|}\left[\tfrac{1}{2}\sum_{n'}(f_{n'}^*p_{n+n'}+f_{n'}p_{n'-n}^*)+d_n+\delta_{n,0}\right]\ . \tag{3.7e}$$

The parameter α_n is defined as $\alpha_n = n\alpha_1$, where $\alpha_1 \equiv 2\pi c/\mathscr{L}$ is the intermode spacing.

The stationary solutions of Eqs. (3.7) are labeled by the same index j as Eqs. (2.13) and have the form

$$f_n^{(j)} = [2C - (1+\tilde{\Delta}_j^2)]^{1/2}\delta_{n,j} , \tag{3.8a}$$

$$p_n^{(j)} = -f_n^{(j)} \frac{1 - i\tilde{\Delta}_j}{1+\tilde{\Delta}_j^2 + |f_n^{(j)}|^2} , \tag{3.8b}$$

$$d_n^{(j)} = -\frac{1+\tilde{\Delta}_j^2}{1+\tilde{\Delta}_j^2 + |f_j^{(j)}|^2}\delta_{n,0} , \tag{3.8c}$$

where $\tilde{\Delta}_j$ is defined by Eq. (2.13b) and $\delta\Omega \equiv \delta\Omega_j = \delta\omega_j - \alpha_j$. We linearize Eqs. (3.7) around the jth stationary solution, i.e., we let

$$X_n = X_n^{(j)}\delta_{n,j} + \delta X_n , \tag{3.9a}$$

with $X_n \equiv (f_n, f_n^*, p_n, p_n^*)$ and

$$d_n = d_n^{(j)}\delta_{n,0} + \delta d_n , \tag{3.9b}$$

and obtain an infinite-dimensional linear system of equations for the fluctuation variables δX_n and δd_n. The matrix of the coefficients of the linear equations can be put in a block-diagonal form by selecting δf_{n+j}, δp_{n+j}, δf_{j-n}^*, δp_{j-n}^*, and δd_n as the coupled fluctuation variables. Thus, for a selected steady state j and for every value of n ($n = 0, \pm 1, \pm 2, \ldots$) we have

$$\dot{\delta} f_{n+j} = i\delta\Omega_j \delta f_{n+j} - \kappa(\delta f_{n+j} + 2C\delta p_{n+j}) , \tag{3.10a}$$

$$\dot{\delta} f_{j-n}^* = -i\delta\Omega_j \delta f_{j-n}^* - \kappa(\delta f_{j-n}^* + 2C\delta p_{j-n}^*) , \tag{3.10b}$$

$$\dot{\delta} p_{n+j} = \gamma_\perp\{\delta f_j^{(j)}\delta d_n + \delta f_{j+n} d_0^{(j)} - [1 + i(\tilde{\Delta}_j - \tilde{\alpha}_n)]\delta p_{n+j}\} , \tag{3.10c}$$

$$\dot{\delta} p_{j-n} = \gamma_\perp\{\delta f_j^{(j)*}\delta d_n + \delta f_{j-n}^* d_0^{(j)} - [1 - i(\tilde{\Delta}_j + \tilde{\alpha}_n)]\delta p_{j-n}^*\} , \tag{3.10d}$$

$$\dot{\delta} d_n = +i\alpha_n \delta d_n - \gamma_{\|}[\tfrac{1}{2}(f_j^{(j)*}\delta p_{n+j} + p_j^{(j)}\delta f_{j-n}^* + f_j^{(j)}\delta p_{j-n}^* + p_j^{(j)*}\delta f_{n+j}) + \delta d_n] . \tag{3.10e}$$

Equations (3.10) form a closed set of linear equations for each value of the integer n. The ansatz

$$\begin{bmatrix} \delta f_{n+j}(t') \\ \delta f_{j-n}^*(t') \\ \delta p_{n+j}(t) \\ \delta p_{j-n}^*(t) \\ \delta d_n(t) \end{bmatrix} = e^{\lambda t'} \begin{bmatrix} \delta f_{n+j}^{(0)} \\ \delta f_{j-n}^{(0)*} \\ \delta p_{n+j}^{(0)} \\ \delta p_{j-n}^{(0)*} \\ \delta d_n^{(0)} \end{bmatrix} , \tag{3.11}$$

leads to a fifth-degree characteristic equation for λ of the form

$$\sum_{i=0}^{5} A_i(\alpha_n)\lambda^i = 0 , \tag{3.12}$$

where the coefficients $A_i(\alpha_n)$ are complicated, but explicit expressions that depend upon the stationary-state parameters as well as the sideband frequency α_n. The steady state which is being probed is stable if and only if $\mathrm{Re}\lambda_i < 0$ for $i = 1,2,\ldots,5$, and for all values of n. The appearance of a positive real part of an eigenvalue for a given value of n is an immediate indication that the selected steady state is unstable against a small perturbation. The instability manifests itself with the growth of sidebands at the frequencies $\pm\alpha_n$; hence, for example, the field amplitude $F(z',t')$ begins to depart from its stationary configuration F_{st} and develops a space and time structure.

Competitive effects between coexisting steady states become especially significant when the intermode spacing α_1 is of the order of a few atomic linewidths or smaller. In this case, unavoidably, the scaled cavity linewidth $\tilde{\kappa} = \kappa/\gamma_\perp$ is considerably smaller than unity (good-cavity limit) because $\tilde{\alpha}_1 = 2\pi\tilde{\kappa}/T$ and $T \ll 1$. Under these conditions, three out of the five eigenvalues tend to have large and negative real parts; the remaining two eigenvalues are

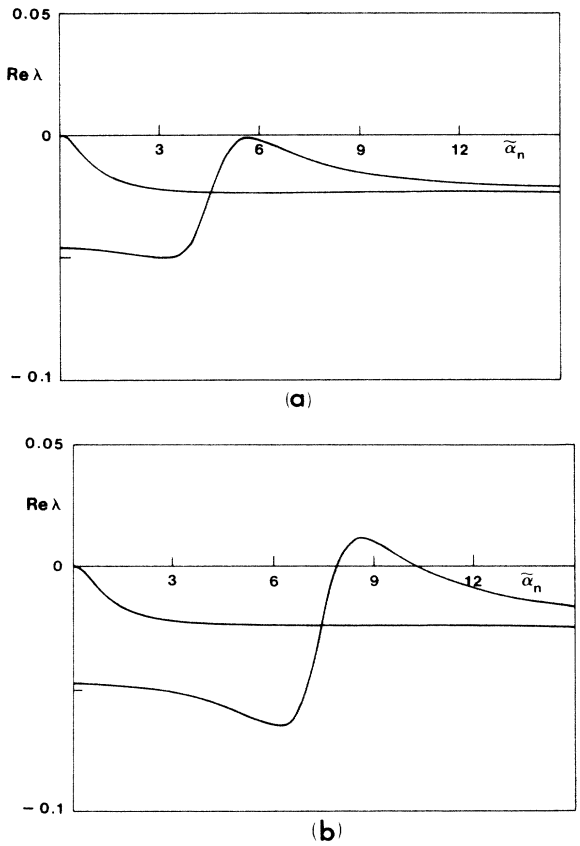

FIG. 2. (a) The two largest real parts of the eigenvalues of the linearized equations (3.10) are plotted as functions of $\tilde{\alpha}_n$ viewed as a continuous variable for $\alpha L = 0.8$, $R = 0.95$, $\tilde{\alpha}_1 = 3$, $\tilde{\gamma} = 1.5$, $\tilde{\delta}_{AC} = 0$. These eigenvalue describe the response of the system around the stationary state $j = 0$ which is stable because $\mathrm{Re}\lambda < 0$ for all values of $\tilde{\alpha}_n$. The other two possible steady states $j = \pm 1$ are both unstable. (b) Same as (a) with $\alpha L = 2$. For a sufficiently high gain, the real part of the amplitude eigenvalue becomes positive and the $j = 0$ steady state becomes unstable in correspondence with $\tilde{\alpha}_3 = 3\tilde{\alpha}_1$. Because the stationary states $j = \pm 1$ are also unstable, the system is expected to develop self-pulsing for sufficiently long times.

responsible for the appearance of unstable behavior for appropriate values of the parameters.[17] Of these two eigenvalues, one has a zero real part for $\tilde{\alpha}_n=0$, and is recognized as the phase eigenvalue; the other can be labeled as the amplitude eigenvalue, for convenience. The distinction between phase and amplitude eigenvalues becomes especially clearcut in the resonant case ($\delta_{AC}=0$) when the set of linearized equations for $j=0$ splits into two parts, one related to the amplitudes and the other to the phases.

It is interesting to compare the behavior of the two relevant eigenvalues in two specific situations. The first one corresponds to a resonant condition ($\delta_{AC}=0$) and to increasing values of the gain parameter $2C$; the second corresponds to a fixed value of the gain and to growing values of the detuning. The resonant situation was already investigated in Refs. 8, 9, and 13, and the results are already known. Typical results are illustrated in Figs. 2(a) and 2(b) where the real parts of the two field eigenvalues are plotted as functions of the scaled sidemode frequency $\tilde{\alpha}_n$ regarded as a continuous variable (note that the only meaningful values of Reλ correspond to values of $\tilde{\alpha}_n$ that are integer multiples of $\tilde{\alpha}_1$). The gain selection in Fig. 2(a) is such that the stationary state $j=0$ is stable. The only other possible stationary states in this case are $j=\pm 1$; these states are unstable so that the system, initially placed in the $j=0$ state, will remain there indefinitely. The gain parameter in Fig. 2(b) is, instead, large enough that the amplitude eigenvalue develops a positive real part in correspondence with the sideband frequency $\tilde{\alpha}_n=3\tilde{\alpha}_1$. In this case, as already predicted in Refs. 8 and 9, oscillations will develop as the system departs from its initial stationary configuration. It is important to remark that in both Figs. 2(a) and 2(b) the phase eigenvalue associated with $j=0$ state maintains a negative real part, so that the appearance of self-pulsing is the result of the destabilization of the field amplitude. This is a general feature of all resonant configurations for the stationary state $j=0$.

In Figs. 3(a) and 3(b) we illustrate the effect of increasing the detuning between the center of the atomic line and ω_C. In both cases, the gain of the system is much smaller than would be required for the appearance of an instability of the type shown in Fig. 2(b). The steady state $j=0$ is stable for the chosen value of $\tilde{\delta}_{AC}$ in Fig. 3(a), but it becomes unstable for the larger detuning value used in Fig. 3(b). Here the instability is associated with the growth of sidebands at $\tilde{\alpha}_n=\tilde{\alpha}_1$. Note, however, that unlike the resonant case, here the instability is brought about by a destabilization of the phase, i.e., by a very different physical mechanism from what is operative in connection with the RNGH instability.[8,9] This feature is also typical of all detuning scans that we have investigated.

We are now in a position to consider the matter of competition among different steady states, and the different scenarios that one may expect from the direct numerical integration of the Maxwell-Bloch equations. If the intermode spacing is so large that only one steady state can satisfy the threshold condition, the situation is not essentially different from that of a single-mode laser: above threshold for laser action the only stationary state is normally stable as long as $\tilde{\kappa}$ is sufficiently small and the gain

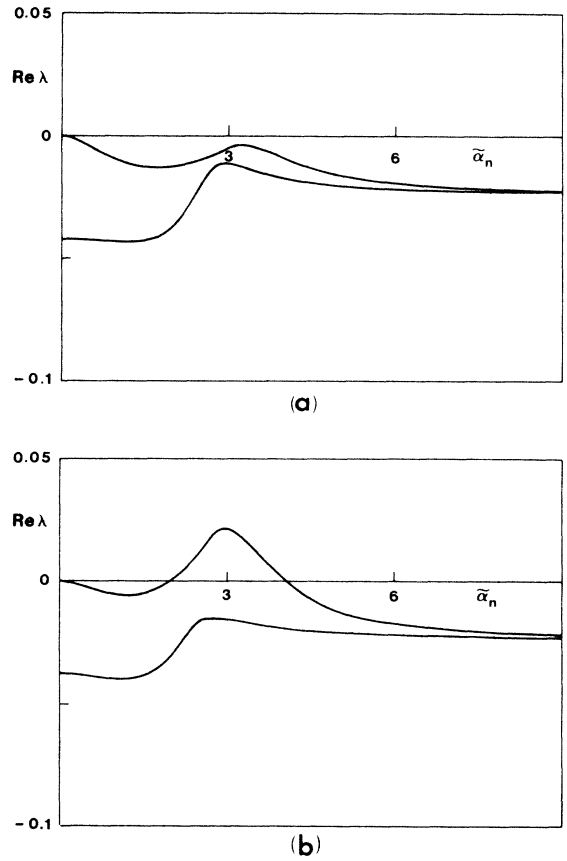

FIG. 3. (a) For increasing values of the detuning parameter, $\tilde{\delta}_{AC}$, the phase eigenvalues eventually develops a positive real part. In this case, the $j=0$ steady state is stable; $\alpha L=0.5$, $R=0.95$, $\tilde{\alpha}_1=3$, $\tilde{\gamma}=0.8$, $\tilde{\delta}_{AC}=0.7$. (b) Same as (a) with $\tilde{\delta}_{AC}=1.2$. In correspondence with these parameters, the stationary state $j=0$ becomes unstable (phase instability); the states $j=\pm 1$ are also unstable, so that pulsations are expected for sufficiently long times.

of the system is lower than the so-called second-laser threshold. For simplicity, we consider now a situation where $\tilde{\alpha}_1$ is of the order of a few $\gamma_\perp$, and the gain is adjusted so that only two coexisting steady states ($j=0, j=1$) can be found over most of the detuning range $(0,\tilde{\alpha}_1)$. In the following discussion, the gain is held constant, while $\tilde{\delta}_{AC}$ is allowed to vary from 0 to α_1 (the situation for negative detuning is symmetric and it involves the stationary states $j=0, j=-1$). For each value of $\tilde{\delta}_{AC}$ we have calculated the eigenvalues of the two stationary states and recorded the range of the $\tilde{\alpha}_n$ axis where Re$\lambda>0$. This range has been plotted as a function of $\tilde{\delta}_{AC}$ in Figs. 4(a) and 4(b) to illustrate the behavior of the domain of instability of the ring laser as a function of the detuning parameter.

Figure 4(a) shows the existence of a detuning range $(0<\tilde{\delta}_{AC}\lesssim 0.8)$ where the stationary state $j=0$ is stable, while $j=1$ is unstable, and a range $(2.2<\tilde{\delta}_{AC}\lesssim 3)$ where the converse is true; here there is no ambiguity with regard to the long-term behavior of a solution. On the other hand, both steady states are unstable for $0.8<\tilde{\delta}_{AC}\lesssim 2.2$ and self-pulsing is expected to develop

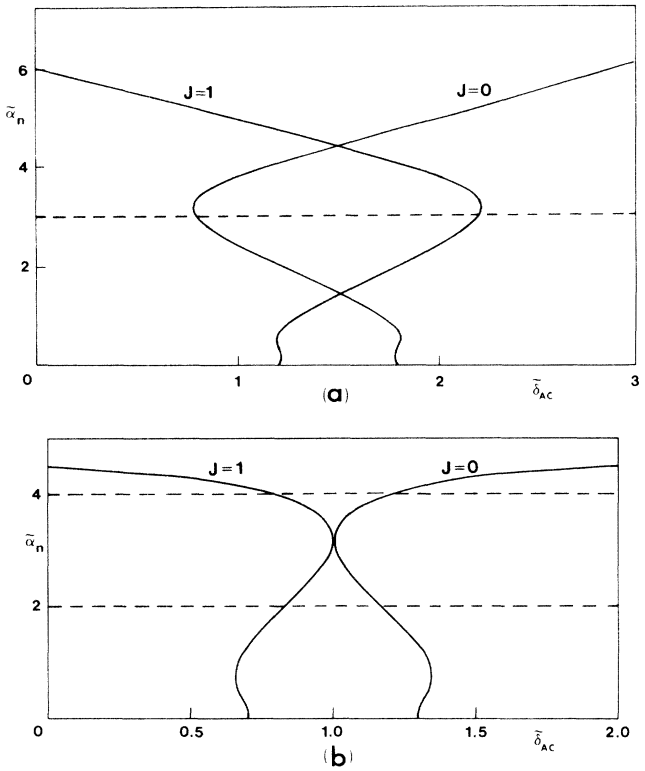

FIG. 4. (a) Instability boundaries for the steady states $j=0$ and $j=1$ as functions of the detuning parameter $\tilde{\delta}_{AC}$. The steady state $j=0$ becomes unstable to the right of the solid line marked $j=0$. The steady state $j=1$ is unstable to the left of the corresponding solid line. The horizontal dashed line marks the position of the first off-resonant cavity mode. The parameters chosen in this calculation are $\alpha L=0.5$, $R=0.95$, $\tilde{\alpha}_1=3$, $\tilde{\gamma}=0.8$. (b) Instability boundaries for the steady states $j=0$ and $j=1$. The steady state $j=0$ becomes unstable to the right of the solid line marked $j=0$. The steady state $j=1$ is unstable to the left of the corresponding solid line. The horizontal dashed lines mark the position of the first two off-resonant cavity modes. The parameters chosen in this calculation are $\alpha L=0.3$, $R=0.95$, $\tilde{\alpha}_1=2$, $\tilde{\gamma}=2$. Over the range $0.85<\tilde{\delta}_{AC}<1.15$ both stationary states $j=0$ and $j=1$ are stable, hence bistability and hysteresis are expected upon scanning the detuning parameter.

under these conditions. This is confirmed by the numerical solution of the Maxwell-Bloch equations as discussed in Sec. IV. In Fig. 4(b) the laser gain has been reduced to a value such that while two possible steady states still exist, their respective domains of instability do not overlap. On the basis of the linearized stability analysis, one then expects the occurrence of discontinuous jumps from one stationary state to the other as the detuning parameter is scanned in a continuous adiabatic way. This conjecture is supported by the numerical analysis disussed in Sec. IV.

In closing, it is worth remarking once again that the instabilities associated with the detuning scans are of a different nature from those investigated in Refs. 8 and 9, and should not be interpreted as RNGH-type instabilities under detuned conditions. Of course, both amplitude and phase instabilities can become operative at the same time for sufficiently high gain, and in the presence of detuning. From an experimental point of view, a phase instability should be more readily accessible to observation because of its reduced demands on the gain of the system.

IV. NUMERICAL SOLUTIONS OF THE MAXWELL-BLOCH EQUATIONS

Before we enter into the details of the numerical analysis of the Maxwell-Bloch equations, it will be useful to restate the main difference between the present calculations and the setting considered in Refs. 8, 9, and 12. In resonance, this system can be described by separate equations for the intensity and the phase of the field, each set being related to a different linearized eigenvalue for the field variable. The eigenvalue that corresponds to the phase is always equal to zero for $\tilde{\alpha}_n=0$, and the one related to the intensity can develop a positive real part for sufficiently large values of the pump parameter. As described in Ref. 8, this seems to indicate that all the energy used to increase the population inversion cannot be transferred to a single mode, but there exists a limit to the pump parameter above which the energy is distributed also to nonresonant cavity modes whose gain can thus be made larger than their losses. At this point, multimode operation of the laser can be obtained in the sense that two or more optical frequencies are excited simultaneously.

In the presence of detuning, the threshold for this type of instability increases because the energy transfer is now less efficient, in agreement with the findings of Zorell.[12] However, the phase eigenvalue can develop a positive real part of its own, even for small values of the pump parameter, as shown in the previous section. This can be interpreted as the onset of an additional choice on the part of the laser system between oscillation at the active mode or at its nearest neighbor. Thus, three types of behavior become possible:

(1) monostability, when the intermode spacing is large enough that the operating mode goes below laser threshold before the adjacent one becomes active;

(2) bistability, if the laser operates in one mode, or its nearest neighbor, but both are stable in their region of coexistence;

(3) dual-mode operation (self-pulsing), if the laser can support both modes simultaneously. In this case, periodic self-pulsing develops at a frequency given by the separation between the adjacent mode-pulled cavity modes. We have called this behavior "phase instability" because the eigenvalue whose real parts become positive is associated with the phase equation in resonance.

These three possibilities will be observed depending on the values of $\tilde{\alpha}_1$, $\tilde{\gamma}$, and $\tilde{\kappa}$. In the case of the CO_2 laser, for example, where $\tilde{\gamma}$ is much smaller than $\tilde{\kappa}$, bistability is the dominant behavior if $\tilde{\alpha}_1$ is sufficiently small for a given gain value. When self-pulsing develops, only limit cycles become possible in the phase space of the dynamical variables because the pulsations are the result of a beating effect between two separate modes. Of course, this possibility cannot exist in the RNGH setting in resonance.

Our method of solving the Maxwell-Bloch equations is

based on the procedure developed in Ref. 8, and suitably adapted to handle the simple extension to complex field and polarization variables. For the convenience of possible future investigators of this problem, we have assembled a number of useful comments and the entire set of discretized equations in Appendix A. Here we limit ourselves to a brief survey of the most relevant results.

The equations to be solved by our numerical code are actually more general than Eqs. (3.4) because they *do not* include the mean-field approximation. In order to take advantage of the results of the linear-stability analysis, however, we have selected parameters that are consistent with the mean-field limit, with only one exception: the dots in Fig. 1 represent the steady-state intensity calculated at the end of the dynamical transient under conditions that are rather removed from the mean-field limit. The agreement with the predicted stationary values is excellent.

We are especially interested in verifying the occurrence of the dynamical scenarios which are suggested by the linear-stability analysis. More complicated unstable behaviors are surely possible for different values of the control parameters, but they will be investigated in future studies.

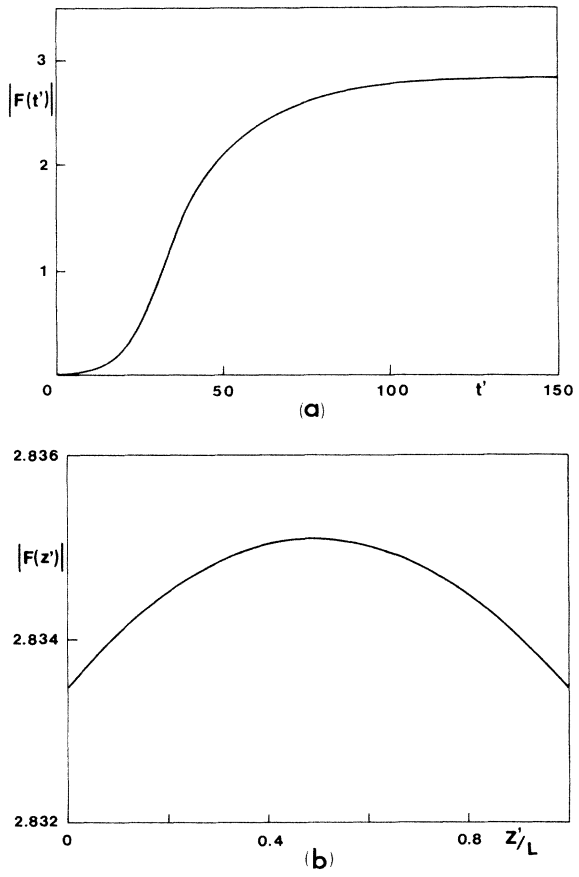

FIG. 5. (a) Time evolution of the modulus of the output field $|F(t')|$, from an initial small value. The parameters used in this simulation are identical to those used in Fig. 4(a) with $\tilde{\delta}_{AC}=0.5$. As expected, the system evolves to the stationary state $j=0$. (b) Spatial profile of the field modulus $|F(z')|$ plotted as a function of the scaled longitudinal coordinate z'/L. The field intensity $|F(z')|^2$ is very nearly uniform everywhere under the mean-field conditions.

The approach to a stationary state or the appearance of self-pulsing under the expected conditions is illustrated in Figs. 5 and 6. Figure 5(a) displays the evolution of the output-field modulus $|F|$ for a detuning value that lies to the left of the $j=0$ instability boundary [see Fig. 4(a)]. As expected, starting from a very small initial field, the laser evolves into a constant intensity state, in excellent agreement with the prediction of Eq. (2.13a). The real and imaginary parts of the field in steady state are expected to undergo a sinusoidal oscillation with a frequency

$$\frac{\delta\omega_0}{\gamma_\perp}=\tilde{\delta}_{AC}-\tilde{\Delta}_0 .$$

This, also, has been verified to excellent accuracy. The very high degree of longitudinal uniformity which is expected for the chosen parameters is confirmed by Fig. 5(b).

Upon increasing the detuning beyond the value $\tilde{\delta}_{AC}\approx 0.8$ output, pulsations begin to appear. An example of fully developed oscillations is shown in Fig. 6(a) for $\tilde{\delta}_{AC}=1.2$. As expected, because of the nonlinearity of the Maxwell-Bloch equations, the intensity modulation is not exactly sinusoidal. On the other hand, the output oscillations are the result of competition between two coexisting steady states, so that the fundamental pulsation frequency ought to be rather close to the beat note between the $j=0$ and $j=1$ steady states. This argument is well supported both by a direct reading of the frequency oscillation from Fig. 6(a) and by the output heterodyne spectrum as shown in Fig. 6(b).

We note in this connection that spectral studies of dynamical phenomena provide a very useful complement to the time-dependent solutions of differential equations. Theoretical studies, for the most part, have relied on homodyne spectral techniques, while experimental investigations have focused typically on heterodyne spectra. Because the latter technique offers considerably greater insight into the dynamical mechanisms that generate the observed oscillations, we have modified a conventional fast Fourier-transform code in order to simulate the superposition of the optical laser field of interest with that of a stable reference oscillator. An outline of this procedure is presented in Appendix B.

On increasing $\tilde{\delta}_{AC}$ beyond the value $\tilde{\delta}_{AC}\approx 2.2$ the intensity pulsations disappear and the output field acquires, again, a time-independent amplitude. At this point, the frequency of oscillation of the real part of the solution corresponds to the $j=1$ stationary state.

The appearance of hysteretic effects is nicely displayed by a simulated detuning scan corresponding to the parameters used in Fig. 4(b). In this scan we have used the final configuration of a given calculation as initial conditions for a new calculation corresponding to a slightly larger (or smaller) value of the detuning. The results are displayed in Fig. 7. The vertical arrows in Figs 7(a) and 7(b) indicate the detuning values where the output field is expected to undergo a transition from a lower (higher) intensity level to a higher (lower) one. In practice, the switching threshold is difficult to approach in numerical experi-

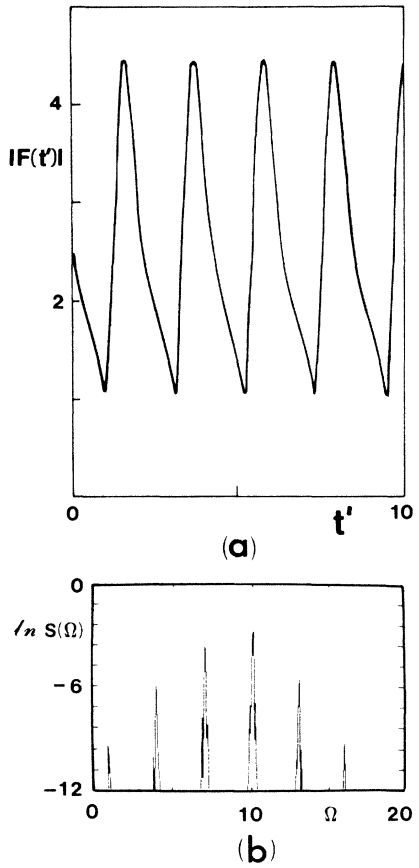

FIG. 6. (a) Long-term time evolution of the modulus of the output field $|F(t')|$. The parameters used in this simulation are identical to those used in Fig. 4(a) with $\tilde{\delta}_{AC}=1.2$. The system evolves into a self-pulsing state as one expects from the results of the linearized analysis. (b) The heterodyne spectrum of the output field mixed with a local oscillator whose optical carrier is removed from ω_c by an amount $10\gamma_\perp$; the spectrum shows the presence of two fundamental oscillation frequencies $\omega^{(0)}=9.986$ and $\omega^{(1)}=7.005$, which are easily traced to the oscillation frequencies associated with the unstable states $j=0$ and $j=1$ [see Eqs. (2.13b) and (2.13c)].

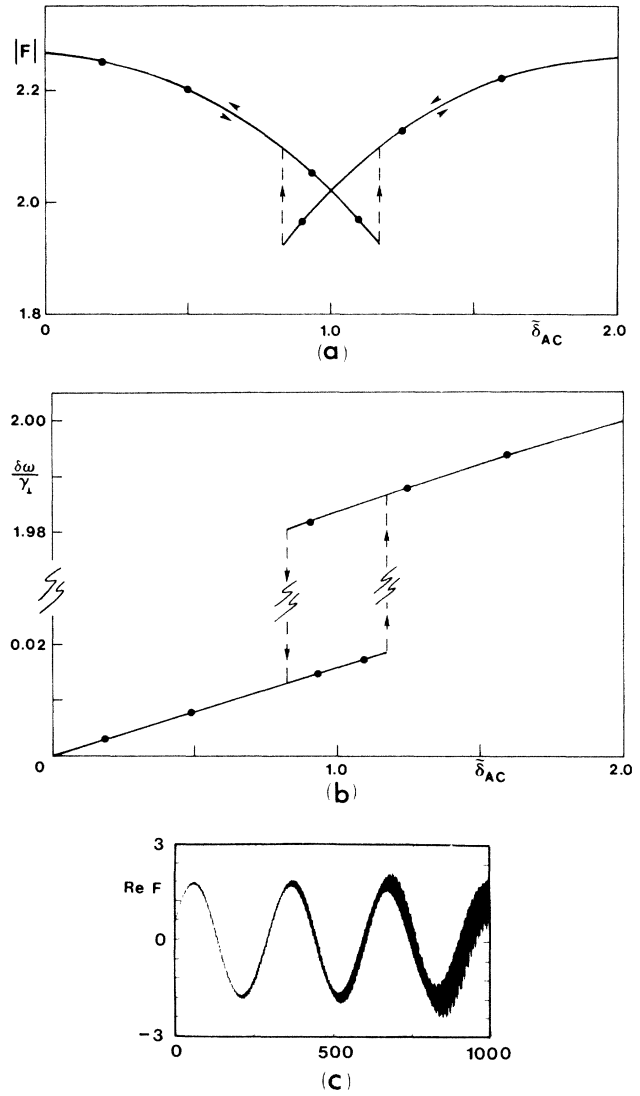

FIG. 7. Simulated detuning scan corresponding to the parameters of Fig. 4(b) ($\alpha L=0.3$, $R=0.95$, $\tilde{\alpha}_1=2$, $\tilde{\gamma}=2$); (a) variation of the output intensity. The dots represent the steady-state values calculated numerically. The solid line is a plot of the modulus of the output field according to Eq. (2.13a); (b) variation of the frequency $\delta\omega_j/\gamma_\perp$ of the output field. The dots represent measurements of the frequency obtained from the numerical solution of the real part of the output field. The solid line is a plot of Eq. (2.13c). (c) The real part of the electric field during the switching period from one steady state to the other.

ments because of critical slowing down. However, it is instructive to follow the evolution of a solution whose initial conditions corresponds to a steady-state configuration on one side of the switching threshold, while the detuning parameter lies on the opposite side. In this case, a long initial transient with a very nearly constant output intensity and optical frequency is followed by a slow transition period when the output intensity switches over to the new stable value and the oscillation frequency acquires the value that is appropriate to the new operating state. The transition state is characterized by a modulation of the output intensity [Fig. 7(c)] at the beat frequency of the adjacent dressed modes which grows to a maximum and then steadily decreases to zero. Clearly, the switchover is characterized by a temporary coexistence of both oscillating modes.

Some of the above theoretical predictions have been observed experimentally in tests carried out with a multimode, homogeneously broadened CO_2 laser, as we discuss in Sec. V.

V. FREQUENCY AND INTENSITY BISTABILITY IN cw CO_2 LASERS

The theoretical results derived in the previous sections apply in a general way to homogeneously broadened lasers such as ruby, dye lasers, Nd:YAG (yttrium aluminum garnet), CO_2, molecular far infrared, and semiconductor

lasers. Of course, these devices operate under very different conditions, so that with a single laser we would not expect to observe but a small fraction of the predicted behaviors. On the whole, the most promising systems for the type of studies discussed in this paper are the far-infrared lasers because of their flexibility with regard to the choice of values of $\tilde{\gamma}$ and $\tilde{\kappa}$. Semiconductor, Nd:YAG and CO_2 lasers, however, are widely used at the present time. They all share a common feature; the population relaxation rate is smaller than the escape rate of radiation out of the cavity ($\gamma_{\parallel} < \kappa$).

As indicated in the theoretical analysis, the output intensity is expected to display a behavior similar to that of Fig. 1(a), when the intermode spacing α_1 is sufficiently large and the gain low enough, so that only one mode at a time has a nontrivial steady state. If two or more steady states coexist, mode-mode competition can yield results that are not accessible to the single-mode theory. Until now it has been generally accepted that homogeneously broadened lasers behave as intrinsically single-mode devices and that their output intensity and operating frequency are determined by the cavity mode that lies nearest to the atomic resonance. In Fig. 8 we show the real parts of the linearized eigenvalues corresponding to the $j=0$, 1, and -1 steady states for $\tilde{\delta}_{AC}=0$, $\tilde{\alpha}_1=3$, $\alpha L=0.3$, $R=0.86$, $\tilde{\kappa}=0.1$, and $\tilde{\gamma}=10^{-3}$. With these operating parameters, all three steady states correspond to nontrivial stable solutions, as shown by the eigenvalues. The actual output intensity and operating frequency of the laser obviously depend on the previous history of the device. In fact, if we carry out a detuning scan along the lines of Fig. 4, we see that the $j=0$ steady state becomes unstable only for values of $\tilde{\delta}_{AC}$ which are larger than $\tilde{\alpha}_1$. This suggests that, upon detuning the cavity from the center of the atomic line, the operating mode will maintain control of the laser output even if other possible steady states have a higher unsaturated gain and are actually closer to the center of the atomic line. Strictly speaking, the choice of the intermode spacing ($\tilde{\alpha}_1=3.0$) is not consistent with the value $\tilde{\kappa}=0.1$ in the mean-field limit, i.e., the relation $\kappa=|\ln R|\,\tilde{\alpha}_1/2\pi$ is not satisfied. The value of $\tilde{\kappa}$ considered here is larger than prescribed by this formula because it simulates the presence of the additional losses due to the intracavity modulator. The results of this analysis give a good qualitative indication of the behavior of a real system, as we have verified using a CO_2 laser with more than one mode under the gain curve. Our experiments have been carried out using the setup schematically shown in Fig. 9. The cavity tuning is controlled by a PZT (lead zirconium titanate) driver mounted on one of the mirrors, while the level of internal losses is set with an electro-optic modulator. The total gas pressure inside the tube was varied from 13 to 20 Torr to allow some variation of the width of the gain curve. The total length of the ring cavity was about 2 m.

In Fig. 10 we show the output intensity as a function of the voltage applied to the PZT. At low values of the pressure and small cavity losses, the output intensity grows monotonically from zero to a maximum value and then decreases to zero again [Fig. 10(a)]. After increasing the pressure to 20 Torr and raising the value of the cavity losses, we note a discontinuous jump in the intensity as we vary the position of the mirror M. The increase in pressure is responsible for the emergence of more than one possible steady-state solution; on detuning the position of the cavity, the laser output follows the operating mode until the losses exceed the gains. At this point, the observed intensity jumps to the value corresponding to the steady state that has the highest gain; if this lies around the center of the gain curve, the output intensity undergoes jumps from the noise level to its maximum value [Fig. 10(b)]. The voltage scans were carried out at different rates to verify the independence of our results on the slow temporal variations of the operating parameters. In fact, on occasions we have stopped the voltage scans altogether to verify that the output intensity did not vary from the observed values.

In order to provide more conclusive evidence that the observed switching of the intensity corresponds to a

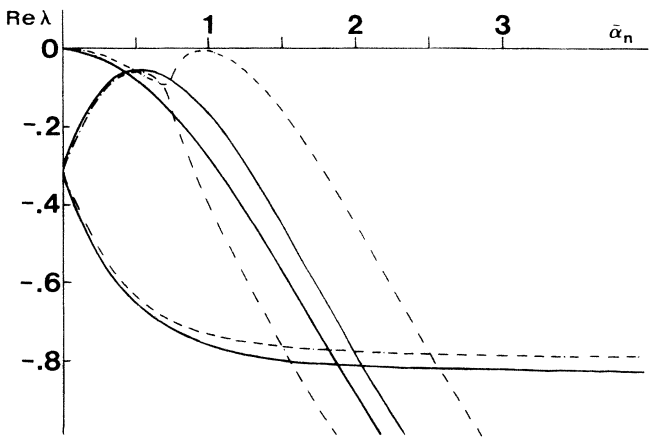

FIG. 8. The three largest real parts of the eigenvalues λ as functions of $\tilde{\alpha}_n$ viewed as a continuous variable for $\alpha L=0.3$, $R=0.86$, $\kappa=0.1$, $\tilde{\alpha}_1=3.0$, $\tilde{\gamma}=10^{-3}$, and $\tilde{\delta}_{AC}=0$ for the stationary states $j=0$ (solid line) and $j=1$ (dashed lines). These states are stable even if the atomic transition is resonant with the selected cavity mode.

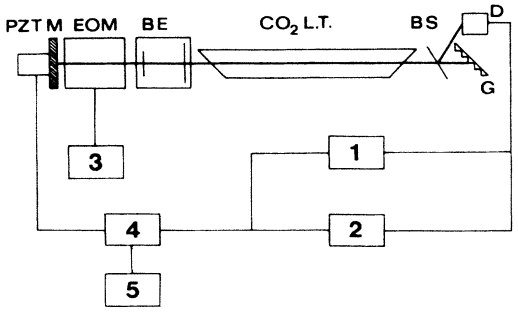

FIG. 9. Experimental setup: PZT, piezoelectric ceramic; M, total reflectors; EOM, electro-optic modulator; BE, beam expander; BS, beam splitter; G, grating; D, Hg CdTe detector; 1, X-Y oscilloscope; 2, graphic recorder; 3 and 4, HV power supplier; 5, wave-function generator.

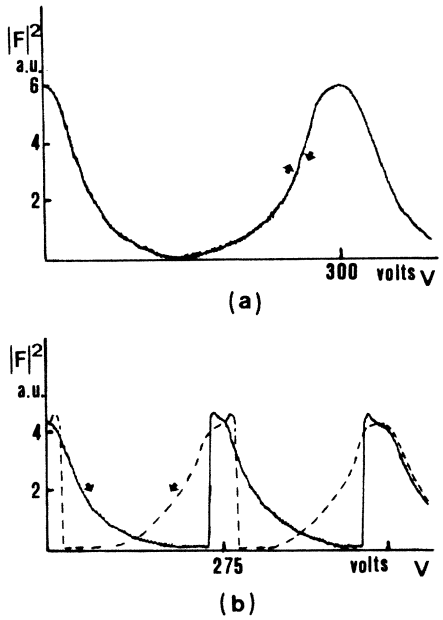

FIG. 10. Output intensity as a function of the voltage applied to the PZT(V). (a) At a pressure of 8 Torr and with no voltage applied to the EOM ($V_0=0$). This configuration corresponds to the minimum losses. (b) At a pressure of 20 Torr and $V_0=250$ V. The maximum loss value accepted by the system corresponds to $V_0=1100$ V. The solid (dashed) line represents the forward (backward) voltage scan.

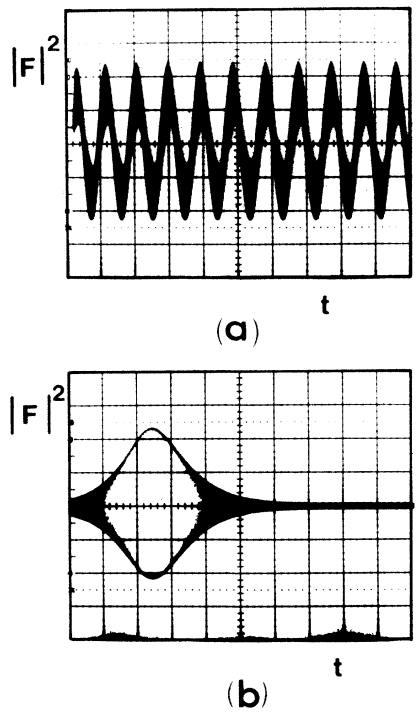

FIG. 11. Output intensity as a function of time during the discontinuous jump observed in Fig. 10(b). (a) Time scale: 20 nsec/div. The observed oscillations corresponds to the beating between two adjacent modes. (b) Time scale: 10 μsec/div. The duration of this transient is approximately 50 μsec, which is comparable with $\gamma_{\parallel}^{-1}$.

change in the operating mode, we have analyzed the transient regime during the transition process and observed a beat pattern with a frequency of about 60 MHz [Fig. 11(a)]; this value is consistent with the frequency spacing between neighboring mode-pulled lines and in good agreement with the theoretical result shown in Fig. 7. On the other hand, the duration of the transient of about 50 μsec, which can be observed in Fig. 11(b), is also consistent with the results of the numerical simulations which indicate that this transient should last about a decay time $\gamma_{\parallel}^{-1}$ of the population inversion.

In typical CO_2 lasers the gain width ranges from 50 to 100 MHz, the cavity modes are separated by 50—150 MHz and the unsaturated gain is about twice as large as the threshold value. Under these conditions, the output intensity decays to zero during a detuning scan before the system jumps to another operating frequency. However, in Nd:YAG lasers where the intermode spacing is much smaller than $\gamma_{\perp}$, the behavior of the output intensity is expected to be similar to that displayed in Fig. 7, and the intensity jumps should be less pronounced than with CO_2 lasers.

The results of these tests confirm the existence of bistability in the variation of the output intensity and of the operating frequency as one scans the detuning parameter $\tilde{\delta}_{AC}$, in qualitative agreement with the theoretical predictions. Furthermore, they show that a homogeneously broadened laser, even if it operates in a single mode, may not function at the mode which lies nearest to the center of the atomic line.

ACKNOWLEDGMENTS

This research has been partially supported by a contract with the U.S. Army Research Office (Durham, NC), a grant from the National Science Foundation (Washington, D.C.), a grant from the Italian National Research Council (Consiglio Nazionale delle Ricerche), and a North Atlantic Treaty Organization (NATO) travel grant. This work has been carried out in the framework of an operation launched by the Commission of the European Communities under the experimental phase of the European Community Stimulation Action. We are grateful to the CO_2-laser group of the Istituto Nazionale di Ottica and especially to Professor F. T. Arecchi for providing the necessary equipment for the experiments and for useful discussions about these results.

APPENDIX A

The starting point of our numerical analysis is given by the equations of motion

$$\frac{\partial \mathcal{F}}{\partial z}+\frac{1}{c}\frac{\partial \mathcal{F}}{\partial t}=-\alpha \mathcal{P} , \tag{A1a}$$

$$\frac{\partial \mathcal{P}}{\partial t}=\gamma_{\perp}[\mathcal{F}\mathcal{D}-(1+i\tilde{\delta}_{AC})\mathcal{P}] , \tag{A1b}$$

$$\frac{\partial \mathcal{D}}{\partial t}=-\gamma_{\parallel}[\tfrac{1}{2}(\mathcal{F}^{*}\mathcal{P}+\mathcal{F}\mathcal{P}^{*})+\mathcal{D}+1] , \tag{A1c}$$

and by the boundary conditions

$$\mathcal{F}(0,t)=R\mathcal{F}(L,t-(\mathcal{L}-L)/c)\ . \tag{A2}$$

In the reference system (3.1) and in terms of the new variables (3.2), the equations of motion take the form

$$\frac{\partial F}{\partial t'}+\frac{cL}{\mathcal{L}}\frac{\partial F}{\partial z'}=-\kappa(F+2CP)\ , \tag{A3a}$$

$$\frac{\partial P}{\partial t'}=\gamma_{\perp}[FD-(1+i\tilde{\delta}_{AC})P]\ , \tag{A3b}$$

$$\frac{\partial D}{\partial t'}=-\gamma_{\parallel}\left[(PF^*+P^*F)\exp\left[\frac{2z'}{L}\,|\ln R|\,\right]+D+1\right]\ . \tag{A3c}$$

Our discretization scheme is identical to the one adopted by Risken and Nummedal in Ref. 8, apart from a few minor modifications to account for the complex nature of the electric-field amplitude and of the atomic polarization.

The first space and time derivatives are discretized at every grid point (m,n) according to the Taylor expansion formulas

$$\frac{\partial X(m,n)}{\partial z'}=\frac{X(m,n)-X(m-1,n)}{\Delta z'}+\frac{1}{2}\Delta z'\frac{\partial^2 X(m,n)}{\partial z'^2}\ , \tag{A4a}$$

$$\frac{\partial X(m,n)}{\partial t'}=\frac{X(m,n+1)-X(m,n)}{\Delta t'}-\frac{1}{2}\Delta t'\frac{\partial^2 X(m,n)}{\partial t'^2}\ , \tag{A4b}$$

where the second space and time derivatives are to be constructed directly from the equations of motion. The elementary step size $\Delta z'$ is chosen equal to $(cL/\mathcal{L})\Delta t'$. After considerable algebra, the discretized equations take the form

$$F(m,n+1)=a_1F(m,n)+a_2F(m-1,n)+a_3P(m,n)+a_4P(m-1,n)+a_5D(m,n)F(m,n)\ , \tag{A5a}$$

$$P(m,n+1)=b_1P(m,n)+b_2D(m,n)F(m,n)+b_3D(m,n)P(m,n)+b_4D(m,n)F(m-1,n)+b_5P^*(m,n)F^2(m,n)E(m)+b_6P(m,n)F(m,n)F^*(m,n)E(m)+b_7F(m,n)\ , \tag{A5b}$$

$$D(m,n+1)=c_1D(m,n)+\mathrm{Re}[c_2F^*(m,n)P(m,n)E(m)]+c_3P^*(m,n)P(m,n)E(m)+\mathrm{Re}[c_4F(m-1,n)P^*(m,n)E(m)]+c_5D(m,n)F^*(m,n)F(m,n)E(m)+c_6\ , \tag{A5c}$$

where

$$a_1=\tfrac{1}{2}(\Delta\tau)^2\tilde{\kappa}^2\ ,$$
$$a_2=1-\tilde{\kappa}\Delta\tau\ ,$$
$$a_3=-\tfrac{1}{2}2C\tilde{\kappa}\Delta\tau[1-\Delta\tau(1+i\tilde{\delta}_{AC})-\Delta\tau\tilde{\kappa}]\ ,$$
$$a_4=-\tfrac{1}{2}\Delta\tau(2C\tilde{\kappa})\ ,$$
$$a_5=-\tfrac{1}{2}(\Delta\tau)^2(2C\tilde{\kappa})\ ;$$

$$b_1=1-(1+i\tilde{\delta}_{AC})\Delta\tau+\tfrac{1}{2}(1+i\tilde{\delta}_{AC})^2\Delta\tau^2\ ,$$
$$b_2=\tfrac{1}{2}\Delta\tau[1-\Delta\tau(1+i\tilde{\delta}_{AC}+\tilde{\gamma}+\tilde{\kappa})]\ ,$$
$$b_3=-\tfrac{1}{2}(\Delta\tau)^2(2C\tilde{\kappa})\ ,$$
$$b_4=\tfrac{1}{2}\Delta\tau\ ,$$
$$b_5=-\tfrac{1}{4}(\Delta\tau)^2\tilde{\gamma}\ ,$$
$$b_5=-\tfrac{1}{4}(\Delta\tau)^2\tilde{\gamma}\ ,$$
$$b_6=b_5\ ,$$
$$b_7=-\tfrac{1}{2}(\Delta\tau)^2\tilde{\gamma}\ ;$$

$$c_1=1-\tilde{\gamma}\Delta\tau+\tfrac{1}{2}(\Delta\tau)^2\tilde{\gamma}^2\ ,$$
$$c_2=\tfrac{1}{2}(\Delta\tau)^2\tilde{\gamma}(1+i\tilde{\delta}_{AC})+\tfrac{1}{2}\Delta\tau\tilde{\gamma}+\tfrac{1}{2}(\Delta\tau)^2\tilde{\gamma}\tilde{\kappa}+\tfrac{1}{2}(\Delta\tau)^2\tilde{\gamma}^2-\tilde{\gamma}\Delta\tau\ ,$$
$$c_3=\tfrac{1}{2}(\Delta\tau)^2\tilde{\gamma}2C\tilde{\kappa}\ ,$$
$$c_4=-\tfrac{1}{2}\Delta\tau\tilde{\gamma}\ ,$$
$$c_5=-\tfrac{1}{2}(\Delta\tau)^2\tilde{\gamma}\ ,$$
$$c_6=\tfrac{1}{2}(\Delta\tau)^2\tilde{\gamma}^2-\tilde{\gamma}\Delta\tau\ ,$$

where

$$\Delta\tau=\gamma_{\perp}\Delta t',\quad \tilde{\kappa}=\kappa/\gamma_{\perp}$$

and

$$\tilde{\gamma}=\gamma_{\parallel}/\gamma_{\perp}\ .$$

If M is the maximum number of intervals into which the active medium is divided, the boundary conditions are enforced by setting $X(0,n)=X(M,n)$ in the $m=1$ entry of the m loop. The selection of M and of the time step $\Delta\tau$ is constrained by the requirement $2\pi/\tilde{\alpha}_1=M\Delta\tau$.

APPENDIX B: HETERODYNE SPECTRA OF THE OUTPUT FIELD

The heterodyne spectrum of an electromagnetic signal is obtained by superposing the field of interest with a reference field with a fixed amplitude and carrier frequency. We denote by

$$E_0(t)=\mathscr{E}_0(t)e^{-i\omega_c t}+\mathscr{E}_0^*(t)e^{i\omega_c t} \tag{B1a}$$

and

$$E_R(t)=Ae^{-i\omega_R t}+A^*e^{i\omega_R t} \tag{B1b}$$

the optical laser field and the reference signal, respectively. $\mathscr{E}_0(t)$ is the slowly varying complex amplitude, ω_c is the selected cavity frequency, and ω_R is the carrier frequency of the reference signal. The total intensity at the detector is given by

$$I_T(t)=2[\,|A|^2+|\mathscr{E}_0(t)|^2+\mathscr{E}_0(t)A^* e^{-i(\omega_c-\omega_R)t} + \mathscr{E}_0^*(t)Ae^{i(\omega_c-\omega_R)t}]\,. \tag{B2}$$

The power spectrum of the real, time-dependent function $I_T(t)$ consists of three distinct contributions: (i) a δ function centered at zero frequency, (ii) the homodyne spectrum of the field of interest, (iii) the spectrum that results from the beating of the two signals (heterodyne component).

In our simulation the constant background term $2|A|^2$ is subtracted out. The heterodyne part of the spectrum is enhanced by selecting a sufficiently large amplitude for the reference signal, and a large enough detuning $(\omega_c-\omega_R)$ so that the spectral lines of interest are well removed from the origin of the frequency axis. Of course, $(\omega_c-\omega_R)$ cannot be made too large for the following reason: the time-dependent solution $\mathscr{E}(t)$ of the Maxwell-Bloch equations is represented by a string of complex numbers calculated at discrete times $t_1,t_2,\ldots$ spaced by a constant interval Δt. If we are to sample the beat signal with enough accuracy [e.g., by collecting about 10 points per period $T=2\pi/(\omega_c-\omega_R)$], it is clear that the optimal sampling interval $(\Delta t)_{\rm opt}$ should be of the order of $0.1T$. Thus, the frequency detuning should be selected with these two requirements in mind: (i) adequate separation of the spectral lines from the origin of the frequency axis, (ii) accurate sampling of the oscillating beat signal. In our work, the power spectrum of $I_T(t)-2|A|^2$ has been calculated by a standard fast Fourier-transform technique.

---

*Permanent address: Istituto Nazionale di Ottica, Largo Enrico Fermi 6, I-50125 Firenze, Italy.

[1]W. E. Lamb, Jr., Phys. Rev. A **134**, 1429 (1964).

[2]H. Haken, in *Handbuch der Physik,* edited by L. Genzel (Springer-Verlag, Berlin, 1970), Vol. XXV/2c.

[3]M. Sargent III, M. O. Scully, and W. E. Lamb, Jr., *Laser Physics* (Addison-Wesley, Reading, 1974).

[4]Comprehensive surveys of recent advances can be found in the following articles: (a) W. Brunner, R. Fisher, and H. Paul, J. Opt. Soc. Am. B **2**, 202 (1985); (b) L. W. Hillman, J. Krasinski, K. Koch, and C. R. Stroud, Jr., *ibid.*, p. 211; (c) F. Hollinger and Chr. Jung, *ibid.*, p. 218; (d) P. A. Khandokhin and Ya. I. Khanin, *ibid.*, p. 225; (e) L. A. Kotomtseva, N. A. Loiko, and A. M. Samson, *ibid.*, p. 218; (f) T. E. Rozzi and K. A. Shore, *ibid.*, p. 237. See also references therein.

[5]See, for example, L. W. Casperson, *Laser Physics,* in Vol. 182 of *Lecture Notes in Physics,* edited by J. Harvey and D. Walls, (Springer-Verlag, Berlin, 1983), p. 88; N. B. Abraham, T. Chyba, M. Coleman, R. S. Gioggia, N. J. Halas, L. M. Hoffer, S. N. Liu, M. Maeda, and J. C. Wesson, *ibid.*, p. 107; see also N. B. Abraham, L. A. Lugiato, P. Mandel, L. M. Narducci, and D. K. Bandy, J. Opt. Soc. Am. B **2**, 35 (1985).

[6]L. A. Lugiato, R. J. Horowicz, G. Strini, and L. M. Narducci, Phys. Rev. A **30**, 1366 (1984).

[7]L. A. Lugiato, in *Progress in Optics XXI* (North-Holland, Amsterdam, 1984), p. 71.

[8]H. Risken and K. Nummedal, J. Appl. Phys. **39**, 4662 (1968).

[9]R. Graham and H. Haken, Z. Phys. **213**, 420 (1968).

[10]See, for example, A. Z. Grazyuk and A. N. Oraevskii, in *Quantum Electronics and Coherent Light,* edited by P. A. Miles (Academic, New York, 1964); H. Haken, Z. Phys. **190**, 327 (1966); the link between the laser equations and the simplified equations of hydrodynamics which describe the Rayleigh-Bénard instability was established by H. Haken, Phys. Lett. **53A**, 77 (1975).

[11]In response to a small perturbation, single-mode instabilities require the bad-cavity condition $\kappa>\gamma_\perp+\gamma_\parallel$, where κ is the cavity linewidth and $\gamma_\perp$ and $\gamma_\parallel$ the decay rates of the atomic polarization and population difference, respectively. Single-mode instabilities are ruled out in the good-cavity limit, even under hard-mode excitation as shown by L. W. Casperson (private communication).

[12]J. Zorell, Opt. Comm. **38**, 127 (1981).

[13]P. R. Gerber and M. Buttiker, Z. Phys. B **33**, 219 (1979).

[14]The appearance of a multimode instability driven by the phase eigenvalue was also noted by L. W. Hillman and K. Koch, in *Optical Instabilities, Proceedings of the International Meeting on Instabilities and Dynamics of Lasers and Nonlinear Optical Systems,* edited by R. W. Boyd, M. G. Raymer, and L. M. Narducci (Cambridge University Press, Cambridge, England, 1986), p. 256. These authors, however, have not discussed the possible scenarios that this instability can produce on varying the ratio of the population and polarization decay rates.

[15]The procedure adopted in this section follows L. A. Lugiato, in Ref. 7, p. 83.

[16]L. A. Lugiato and L. M. Narducci, Phys. Rev. A **32**, 1576 (1985).

[17]Using the terminology developed in: V. Benza and L. A. Lugiato, Z. Phys. B **35**, 383 (1979), the dressed atomic modes are always stable, while the dressed field modes are responsible for possible instabilities.